Very High Energy Gamma-ray spectral properties of Mkn 501 from CAT Čerenkov telescope observations in 1997[*]

A. Djannati-Ataï[7], F. Piron[4], A. Barrau[5,**], L. Iacoucci[4], M. Punch[7], J.-P. Tavernet[5], R. Bazer-Bachi[2], H. Cabot[3], L.-M. Chounet[4], G. Debiais[3], B. Degrange[4], J.-P. Dezalay[2], D. Dumora[1], P. Espigat[7], B. Fabre[3], P. Fleury[4], G. Fontaine[4], C. Ghesquière[7], P. Goret[8], C. Gouiffes[8], I.A. Grenier[8,9], S. Le Bohec[4,***], I. Malet[2], C. Meynadier[3], G. Mohanty[4], E. Nuss[3], E. Paré[4], J. Québert[1], K. Ragan[1,†], C. Renault[5], M. Rivoal[5], L. Rob[6], K. Schahmaneche[5], and D.A. Smith[1]

[1] Centre d'Etudes Nucléaire de Bordeaux-Gradignan, France (IN2P3/CNRS)
[2] Centre d'Etudes Spatiales des Rayonnements, Toulouse, France (INSU/CNRS)
[3] Groupe de Physique Fondamentale, Université de Perpignan, France (IN2P3/CNRS)
[4] Laboratoire de Physique Nucléaire des Hautes Energies, Ecole Polytechnique, Palaiseau, France (IN2P3/CNRS)
[5] Laboratoire de Physique Nucléaire et de Hautes Energies, Universités de Paris VI/VII, France (IN2P3/CNRS)
[6] Nuclear Center, Charles University, Prague, Czech Republic
[7] Physique Corpusculaire et Cosmologie, Collège de France, Paris, France (IN2P3/CNRS)
[8] Service d'Astrophysique, Centre d'Etudes de Saclay, France (DAPNIA/CEA)
[9] Université Paris VII, France

Abstract. The BL Lac object Mkn 501 went into a very high state of activity during 1997, both in VHE γ-rays and X-rays. We present here results from observations at energies above 250 GeV carried out between March and October 1997 with the CAT Čerenkov imaging Telescope.

The average differential spectrum between 330 GeV and 13 TeV shows significant curvature and is well represented by $\phi_0 E_{\mathrm{TeV}}^{-(\alpha+\beta \log_{10} E_{\mathrm{TeV}})}$, with:

$$\phi_0 = 5.19 \pm 0.13^{\mathrm{stat}} \pm 0.12^{\mathrm{sys-MC}}$$
$$\quad {}^{+1.66^{\mathrm{sys-atm}}}_{-1.04} \times 10^{-11} \, \mathrm{cm}^{-2}\mathrm{s}^{-1}\mathrm{TeV}^{-1},$$
$$\alpha = 2.24 \pm 0.04^{\mathrm{stat}} \pm 0.05^{\mathrm{sys}}, \quad \mathrm{and}$$
$$\beta = 0.50 \pm 0.07^{\mathrm{stat}} \quad (\text{negligible systematics}).$$

The TeV spectral energy distribution of Mkn 501 clearly peaks in the range 500 GeV–1 TeV. Investigation of spectral variations shows a significant hardness-intensity correlation with no measurable effect on the curvature. This can be described as an increase of the peak TeV emission energy with intensity.

Simultaneous and quasi-simultaneous CAT VHE γ-ray and BeppoSAX hard X-ray detections for the highest recorded flare on 16th April and for lower-activity states of the same period show correlated variability with a higher luminosity in X-rays than in γ-rays.

The observed spectral energy distribution and the correlated variability between X-rays and γ-rays, both in amplitude and in hardening of spectra, favour a two-component emission scheme where the low and high energy components are attributed to synchrotron and inverse Compton (IC) radiation, respectively.

Key words: galaxies: active – galaxies: nuclei – galaxies: BL Lacertae objects: individual: Mkn 501 – gamma rays: observations

1. Introduction

Mkn 501, at $z = 0.034$, is the second-closest BL Lac object and, with Mkn 421 ($z = 0.031$), is one of the two extra-galactic sources thus far detected and confirmed at TeV energies. Its TeV emission was discovered in 1995 by the Whipple observatory group (Quinn et al. 1996) above 300 GeV, at the level of 8% of the TeV flux of the Crab Nebula, and subsequently confirmed by the HEGRA collaboration (Bradbury et al. 1997).

Initially, Mkn 501 had been placed in the radio-selected BL Lac family (Stickel et al. 1991, from 1 Jy BL Lac and S4 radio samples). However, its spectral energy distribution (SED) in recent years resembled typical High-Frequency BL Lac objects (mostly X-ray selected) with the low-energy peak in the EUV/soft X-ray energy band, making it a bright Einstein Slew Survey source (Ciliegi et al. 1995). In fact, it can be considered as being intermediate between the radio- and X-ray bright classes of BL Lac (Lamer & Wagner 1998).

From March to October 1997, Mkn 501 showed dramatic activity in the VHE γ-ray band, exhibiting flares during which

it became up to ~ 8 times brighter than the Crab Nebula (e.g., see Protheroe et al. 1997); i.e., two orders of magnitude brighter than its discovery level.

During the same period, Mkn 501 was also extremely active in the X-ray band as reported by the All Sky Monitor (ASM) on board the *Rossi X-Ray Timing Explorer* (RXTE). In April, high-intensity flares were recorded in the hard X-ray range by RXTE (Lamer & Wagner 1998), BeppoSAX (Pian et al. 1998), and OSSE (Catanese et al. 1997) on board the *Compton Gamma Ray Observatory* (CGRO). The synchrotron peak underwent a shift towards high energies as compared to archival data, shifting to energies of $100\,\mathrm{keV}$. This unprecedentedly high energy made Mkn 501 the most extreme known BL Lac object in the X-ray sky.

This paper is dedicated to the study of detailed spectral properties of this source, based on observations carried out with the CAT Čerenkov imaging telescope above $250\,\mathrm{GeV}$ in 1997.

The next section describes briefly the CAT telescope and its specific event reconstruction method. The data-sample used for this paper and the resulting source light-curve are presented in Sect. 3. Spectra derived for different-activity states are given in Sect. 4 and intensity-hardness correlations are studied in Sect. 5. In Sect. 6 we compare simultaneous and quasi-simultaneous CAT and BeppoSAX data for the highest flare recorded on April 16th to the lower activity states of the 7th and 11th of the same period. In Sect. 7 we discuss results and their implications for proposed emission models. The conclusions are given in Sect. 8.

2. CAT Čerenkov Imaging Telescope

The $17.8\,\mathrm{m}^2$ CAT (Čerenkov Array at Thémis) imaging telescope started operation in autumn 1996 on the site of the former solar plant Thémis (France). A complete description of the CAT telescope can be found in Barrau et al. (1998).

The instrument records Čerenkov light from the particles in cosmic-ray showers. The analysis of the shape and the pointing of the resulting images, as discussed in Le Bohec et al. (1998), takes full advantage of the very-high-definition camera. This latter has a $4.8°$ full field of view which is comprised of a central region of 546 phototubes in a hexagonal matrix spaced by $0.13°$ and 54 surrounding tubes in two "guard rings".

The γ-ray image analysis is based on the comparison of individual events and theoretical average images as a function of impact parameter and energy. Accurate analysis of the longitudinal light profile and lateral width of the shower image is possible thanks to the high-resolution camera. This fitting procedure allows the direction and energy of each γ-ray to be determined with good accuracy: the angular resolution $(0.14°)$ is of the order of the pixel size; when selecting showers with an impact parameter less than $130\,\mathrm{m}$, the energy resolution is about 20%, independent of energy, from approximately $300\,\mathrm{GeV}$ to $15\,\mathrm{TeV}$. At the highest energies, the image tails are cut by the field of view, but the light-profile analysis still permits a good energy estimation.

It should be noted that, in general, for the Atmospheric Čerenkov Technique, there is a systematic uncertainty due to variations in the transparency of the atmosphere. Additional uncertainties due to unmastered detector drifts exist, but are fairly low for CAT, and are monitored within the data (e.g., using muon ring images). A conservative estimate of the overall uncertainty on the absolute energy scale is 20%.

To separate γ-ray initiated shower images from those due to hadronic showers we use the χ^2-like goodness-of-fit parameter given by the above procedure, requiring the probability $P_{\chi^2} > 0.35$, and the pointing angle (which is the angle at the image barycentre between the actual source position and the reconstructed angular origin of the γ ray), $\alpha < 6°$. In addition, only images with more than 30 photo-electrons and whose fourth brightest pixel has more than 3 photo-electrons are selected, in order to eliminate the lowest-energy triggers. These cuts yield a rejection factor of about 200, with a γ-ray efficiency better than 40%. Further details on this specific method can be found in Le Bohec et al. (1998).

3. Data sample

A total of 95.3 hours of data were taken on Mkn 501 (ON), together with 36 hours on control regions (OFF), between March and October 1997. The data used for the analysis were selected by quantitative criteria including clear weather and stable detector operation. The data-set has been further limited to zenith angles $< 44°$, for which the detector calibration studies have been completed. This leaves 57.2^{h} ON and 22.5^{h} OFF data for the analysis presented in the following sections. Fig. 1 shows the nightly flux levels as sampled by CAT above $250\,\mathrm{GeV}$ between March and October, 1997. The average flux was approximately twice that of the Crab Nebula, while the highest flare, recorded on April 16th (γ-ray rate $\sim 16\,\gamma/\mathrm{min}$), reached about 8 times the Crab level with signal-to-background ratios of 2.7 for the flare and 0.68 on average (see Fig. 2a,b).

4. Spectra

4.1. Analysis method

As stated in Sect. 3, observations consist of ON and OFF source runs, the latter being used to estimate the background due to hadronic showers. Since the threshold energy of the telescope increases with zenith angle, ON and OFF data are classified within zenith angle bins (with a width of 0.05 in $\cos\theta_z$). Energy bins have been defined so as to be larger than the telescope's energy resolution. Trigger and cut efficiencies – yielding the effective detection area $\mathcal{A}_{\mathrm{eff}}(E)$ – as well as the energy-resolution function are determined by detailed Monte-Carlo simulations of the telescope response as a function of energy and zenith angle. These simulations have been checked and calibrated on the basis of several observables using the nearly-pure γ-ray signal from the highest flare and muon rings. This will be reported in a forthcoming paper.

The spectra are derived in two steps. First, the number of events passing the cuts within each energy and zenith-angle band is determined for ON and OFF runs. Then, for a given hypothesis on the spectral shape, a maximum-likelihood estimation of the
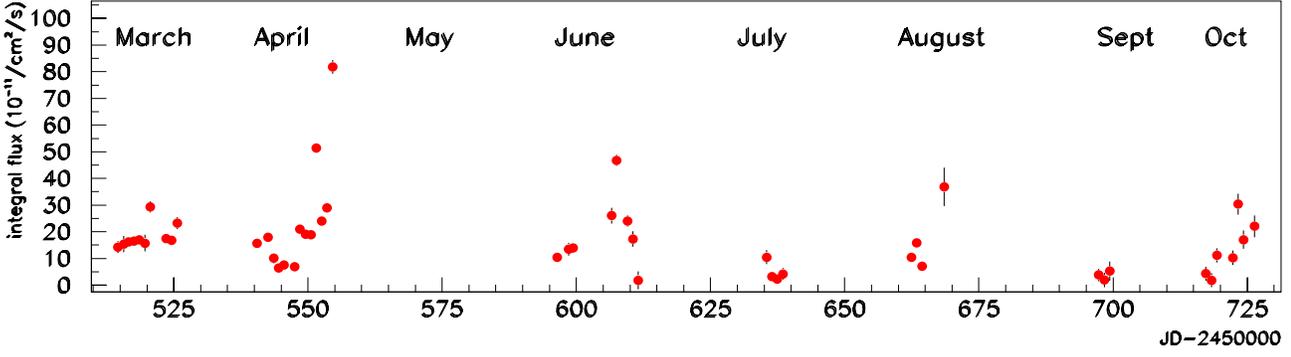
Fig. 1. Mkn 501 nightly integral flux levels above 250 GeV, expressed in units of 10^{-11} cm^{-2}s^{-1}, for observations in 1997. The average spectral shape as derived in Sect. 4 has been assumed in order to estimate the integral flux for observations far from the Zenith.
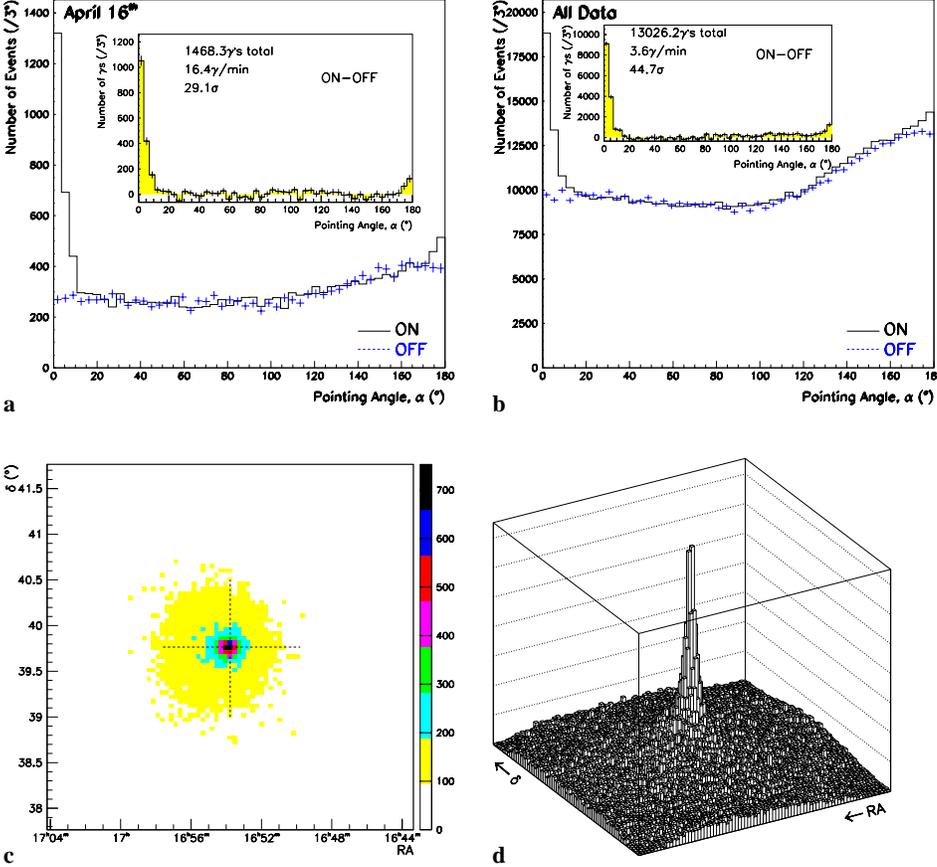

Fig. 2a–d. The Mkn 501 signal seen with the CAT imaging telescope: **a, b** α plots for April 16th and for all data respectively (ON data shown by solid lines, OFF by points with error bars, ON-OFF inset). The signal is clearly seen in the direction of the source (small α), though the direction of some γ-rays is mis-identified, giving a small signal at $\alpha \sim 180°$. **c, d** two representations of the distributions of the reconstructed angular origins for all data (the scales in both plots are identical, the bin size is $0.05°$, no background subtraction has been performed). The cross in **c** marks the position of Mkn 501. Events are selected by the P_{χ^2} (i.e., shape) cut only.

spectral parameters is performed, taking into account the effective area and the energy-resolution function of the telescope.

Two hypotheses have been assumed for the spectral shape: a simple power law ($\mathcal{H}_0$) and a curved shape ($\mathcal{H}_1$). In fact, as we will see below, the data are not compatible with the former shape. The curved shape is suggested by general considerations on emission processes within blazar jets (see Sect. 7.1). Whipple Observatory has also reported a curved shape in terms of a quadratic law in a $\log \phi$ *vs.* $\log E$ representation (Samuelson et al. 1998). We will use the same framework in order to allow for simple comparisons.

To give an estimate of the relevance of $\mathcal{H}_0$ with respect to $\mathcal{H}_1$, the likelihood ratio of the two hypotheses is defined as $\lambda = -2 \times \log \frac{\mathcal{L}(\mathcal{H}_0)}{\mathcal{L}(\mathcal{H}_1)}$. It behaves (asymptotically) like a χ^2 distribution with one degree of freedom.

4.2. Results

In order to investigate spectral variations as a function of source intensity, three independent data-subsets corresponding to different activity states of Mkn 501 – high-intensity flares (HF, integral flux $> 53 \times 10^{-11}$ cm^{-2}s^{-1} above 250 GeV), low-intensity runs (LF, integral flux $< 12 \times 10^{-11}$ cm^{-2}s^{-1}), and

Table 1. Data-subset definition as a function of source intensity. The differential flux is given as $\mathrm{d}\Phi/\mathrm{d}E_{\mathrm{TeV}} = \phi_0 E_{\mathrm{TeV}}^{-(\alpha+\beta\log_{10}E_{\mathrm{TeV}})}$ in units of $10^{-11}\,\mathrm{cm}^{-2}\mathrm{s}^{-1}\mathrm{TeV}^{-1}$. The fit has been done from 330 GeV to 13 TeV. ϕ_0^{pl} and α^{pl} correspond to a simple power-law hypothesis ($\mathcal{H}_0$). λ is the likelihood ratio of the two hypotheses $\mathcal{H}_0$ and $\mathcal{H}_1$. The last two columns give the peak-emission energies $E_{\max} = 10^{\frac{2-\alpha}{2\beta}}$ (in TeV) for the second hypothesis, where for the final column, the values were obtained by re-fitting with β fixed at 0.5.

Set	ON (h)	ϕ_0^{pl}	α^{pl}	ϕ_0	α	β	λ	$E_{\max}$ (GeV)	$E_{\max}^{\beta=0.5}$ (GeV)
LF	13.6	2.72 ± 0.13	2.45 ± 0.05	3.13 ± 0.19	2.32 ± 0.09	0.41 ± 0.17	10.7	410 ± 201	521 ± 82
MF	40.5	4.10 ± 0.10	2.46 ± 0.03	4.72 ± 0.14	2.25 ± 0.05	0.52 ± 0.08	47.1	583 ± 104	563 ± 42
HF	3.1	$14.5\ \pm 0.50$	2.21 ± 0.03	$17.6\ \pm 0.61$	2.07 ± 0.04	0.45 ± 0.09	29.1	840 ± 108	890 ± 77
AV	57.2	4.56 ± 0.10	2.46 ± 0.02	5.19 ± 0.13	2.24 ± 0.04	0.50 ± 0.07	61.5	$578 \pm\ 98$	589 ± 38

mid-intensity flares (MF) – have been established. The average over the complete data-set (AV) has also been considered. The quadratic law used to estimate the spectral parameters is $\phi_0 E_{\mathrm{TeV}}^{-(\alpha+\beta\log_{10}E_{\mathrm{TeV}})}$. Results for each data-subset are given in Table 1. Only statistical errors are quoted in this table.

As noted in Sect. 2, the systematic errors on the absolute energy scale, conservatively estimated at 20%, lead to an error on the absolute flux depending on the spectral index (referred to below as "sys-atm"). Additional errors coming from the limited statistics of the simulated γ-rays (referred to below as "sys-MC") used to determine $\mathcal{A}_{\mathrm{eff}}(E)$ are twofold:

– an overall scaling error which affects the absolute flux.
– possible distortions of $\mathcal{A}_{\mathrm{eff}}(E)$ as a function of energy within the Monte Carlo errors affecting the parameter α. The curvature parameter β is, however, almost unaffected.

Both parameters have proved to be insensitive to modifications of the analysis procedure (which modify efficiencies and energy resolution functions), showing that they are robust.

For the AV spectrum, the complete results are:

$$\phi_0 = 5.19 \pm 0.13^{\mathrm{stat}} \pm 0.12^{\mathrm{sys-MC}}$$
$$\qquad {}^{+1.66^{\mathrm{sys-atm}}}_{-1.04} \times 10^{-11}\,\mathrm{cm}^{-2}\mathrm{s}^{-1}\mathrm{TeV}^{-1},$$
$$\alpha = 2.24 \pm 0.04^{\mathrm{stat}} \pm 0.05^{\mathrm{sys}}, \quad \text{and}$$
$$\beta = 0.50 \pm 0.07^{\mathrm{stat}} \quad \text{(negligible systematics)}.$$

The corresponding covariance matrix for the fit, based on the statistical errors, is:

$$\begin{pmatrix} 0.01767 & -0.00052 & 0.00443 \\ -0.00052 & 0.00168 & -0.00203 \\ 0.00443 & -0.00203 & 0.00475 \end{pmatrix},$$

with α and β being correlated.

The likelihood ratio, λ, for $\mathcal{H}_0$ and $\mathcal{H}_1$ shows that the HF and MF states (and the AV spectrum) have significantly curved shapes: λ has values of 29.1 and 47.1 respectively, corresponding to chance probabilities of 7×10^{-8} and 7×10^{-12} of accepting $\mathcal{H}_1$ were the power-law hypothesis $\mathcal{H}_0$ true. For the LF state, the curvature significance is somewhat lower (a probability of 10^{-3}), but this could be attributed to the weak intensity of the source.

The SEDs are shown in Fig. 3: as can be seen, the VHE peak emission of Mkn 501 clearly takes place in the range
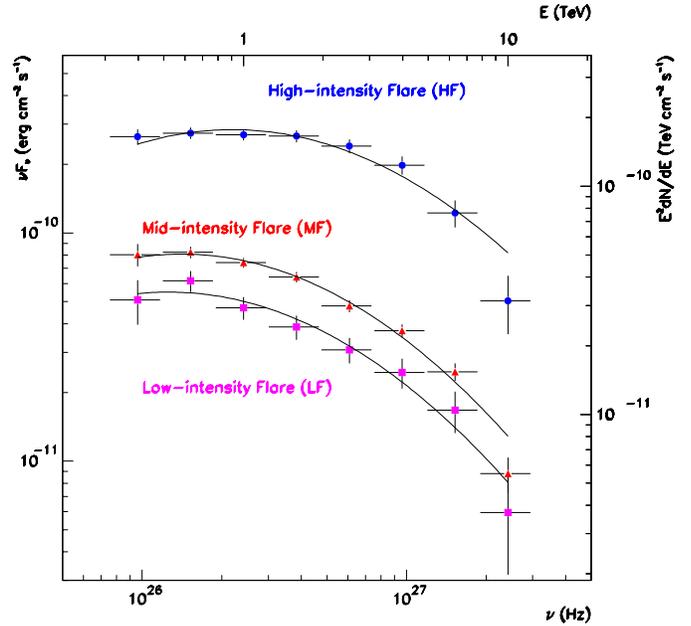
Fig. 3. νF_ν (or $E^2\,\mathrm{d}\Phi/\mathrm{d}E$) spectra for the HF, MF, and LF states. Curves represent the global flux estimated by method described in Sect. 4.1. The points, corresponding to the individual bin intensities, are only indicative and were obtained by the following procedure: The expected number, N_{fit}, of γ-ray events in each energy bin is computed using the fitted flux parameters and taking into account the acceptance and energy resolution functions of the telescope. The observed number of γ-ray events, N_{obs}, is obtained by subtracting ON and OFF data. The ratios $\frac{N_{\mathrm{obs}}}{N_{\mathrm{fit}}}$ give a good approximation of the fluctuation in each bin, and are used to correct the flux values yielded by the fitted curve. Error bars give the combination of uncertainties on N_{obs} and on the effective detection area (statistical only).

of several hundred GeV. The corresponding maximum energy, $E_{\max}$, of the equivalent quadratic form – proportional to $E_{\mathrm{TeV}}^{-2}(E_{\mathrm{TeV}}/E_{\max})^{-\beta\log_{10}(E_{\mathrm{TeV}}/E_{\max})}$ – is given by $E_{\max} = 10^{\frac{2-\alpha}{2\beta}}$ (see Table 1).

There is some indication of an increase in $E_{\max}$ with source intensity, which is equivalently shown by the variation of the fitted values of α. Although the power-law hypothesis is clearly not favoured here, the corresponding variation of α^{pl} values follows the same tendency. On the other hand, the curvature (given by β) is compatible with being constant for the three

Table 2. Hardness-ratio values for five different flux bands (zenith angle $< 25°$). The average integral flux per band above 250 GeV is given in units of 10^{-11} cm^{-2}s^{-1} and has been computed assuming the average spectral shape. Set I corresponds to the highest flare observed on April 16$^{\text{th}}$ and set II to the second-highest flares of April 13$^{\text{th}}$ and June 7$^{\text{th}}$.

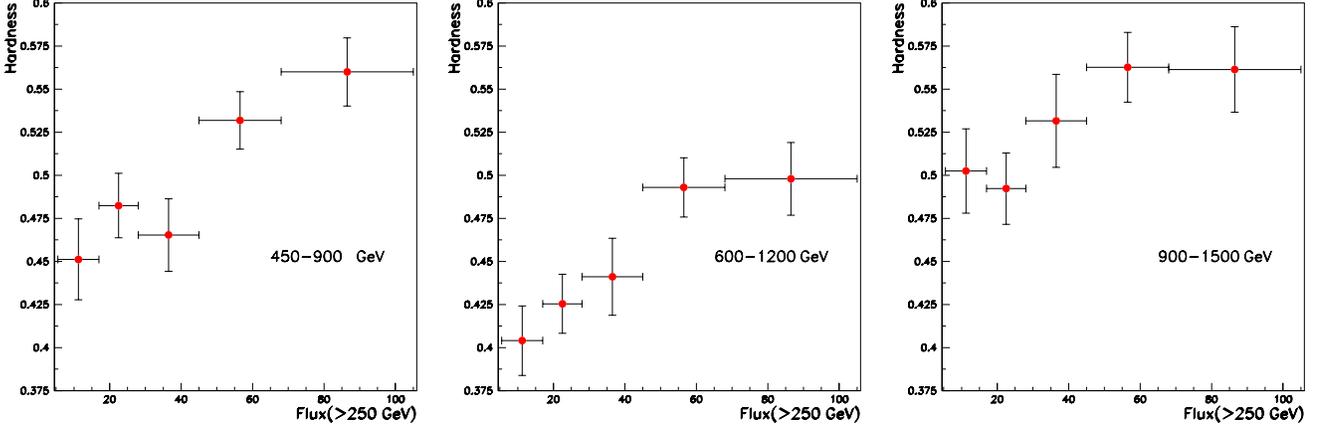| Set	ON (h)	Flux	$R_{[>900/>450]}$	$R_{[>1200/>600]}$	$R_{[>1500/>900]}$
I	1.5	68–105	0.56 ± 0.02	0.50 ± 0.02	0.56 ± 0.03
II	3.5	45–68	0.53 ± 0.02	0.49 ± 0.02	0.56 ± 0.02
III	5.5	28–45	0.47 ± 0.02	0.44 ± 0.02	0.53 ± 0.03
IV	10.5	17–28	0.48 ± 0.02	0.42 ± 0.02	0.49 ± 0.02
V	20.5	5.5–17	0.45 ± 0.02	0.41 ± 0.02	0.51 ± 0.03

Fig. 4. Hardness-ratio values *vs.* source intensity for three different energy bands. Intensities are given as the integral flux above 250 GeV in units of 10^{-11} cm^{-2}s^{-1}.

data-subsets. Fixing $\beta = 0.50$ yields $E_{\max}$ with smaller errors, as shown in the last column of Table 1. This reinforces a possible correlation between intensity and $E_{\max}$. We will investigate this question in more detail in the next section by looking at intensity-hardness correlations.

In order to determine the highest-energy γ-rays measured, the effects of the energy-resolution function and the uncertainty in the absolute energy scale must be taken into account. There is a signal at the 2σ significance level above 12 TeV, after correction for the number of lower-energy events which migrate above this energy due to the energy resolution (and also to the lesser number which migrate to lower energy). Taking into account also the uncertainty in the absolute energy scale implies (conservatively) that there is a 2σ signal above 10 TeV.

5. Spectral hardness vs. source intensity

As compared to a usual spectrum analysis method, a more robust manner to check for spectral changes is to consider two given energies E_{low} and E_{mid}, and the hardness ratio defined as: $R = \frac{N_{E>E_{\text{mid}}}}{N_{E>E_{\text{low}}}}$.

Given the large energy-bins, this ratio is rather insensitive to statistical fluctuations and entails the estimation of only one parameter. Nevertheless, as the detection threshold of atmospheric Čerenkov telescopes increases with zenith angle and is sensitive to slight changes in weather conditions, it is desirable to limit the data-set to low zenith angle runs (here 25°) and choose

E_{low} well above the telescope trigger threshold of 250 GeV (here 450 GeV or above).

Although these two restrictions reduce the available statistics, they allow for minor acceptance corrections by weighting data to normalize them to those taken at the Zenith. This minimizes any possible systematic effects. Furthermore, to achieve the best energy resolution, an additional cut on shower impact parameter (< 130 m at the Zenith) has been introduced.

The limited statistics still forbid a reliable computation of the hardness ratio on a run-by-run (or even night-by-night) basis, except for the highest-intensity runs. Therefore, data have been divided into five sets with different average fluxes. For each data-set in flux, the hardness ratio has been computed for three different energy bands, $[E_{\text{low}}, E_{\text{mid}}]_{\text{GeV}} = \{[450, 900]; [600, 1200]; [900, 1500]\}$, hereafter referred to as $R_{[>900/>450]}$, $R_{[>1200/>600]}$, and $R_{[>1500/>900]}$. The number of hours for each data-set and the corresponding average flux and hardness ratio values are given in Table 2.

As can be seen in Fig. 4, a clear correlation between intensity and hardness is present for all energy-band definitions. The chance probabilities of observing such an effect in the case of an absence of correlation for $R_{[>900/>450]}$, $R_{[>1200/>600]}$ and $R_{[>1500/>900]}$ are respectively: 3.8×10^{-4}, 9×10^{-4}, and 7×10^{-2}. We note that as E_{low} and E_{mid} are raised to higher energies, the significance of the correlation decreases owing to lack of statistics.

Table 3. Observation logs and power output (in units of $10^{-11}\,\mathrm{erg}\cdot\mathrm{cm}^{-2}\mathrm{s}^{-1}$) for BeppoSAX (Pian et al. 1998) and CAT. For CAT, the integral fluxes corresponding to April 7th and 11th are calculated assuming the spectral shape from the LF and MF data-subsets, respectively.

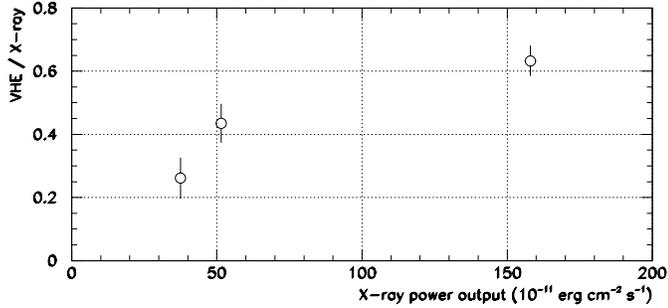| Date	BeppoSAX Observing time (UT)	X-ray power output 13–200 keV	CAT Observing time (UT)	VHE power output 0.25–15 TeV
April 7th	05:30:29 → 16:01:47	37.5 ± 1.5	00:34:06 → 03:56:53	9.8 ± 2.4
April 11th	05:53:57 → 16:25:49	51.5 ± 1.5	01:06:57 → 03:53:16	22.4 ± 3.1
April 16th	03:36:52 → 14:35:48	158.0 ± 2.0	01:42:34 → 03:45:55	100.0 ± 7.5

Fig. 5. The ratio of VHE to X-ray power outputs as a function of the X-ray output, from the data in Table 3. On this plot, a linear relation between the VHE and X-ray intensity would appear as a horizontal line, and a quadratic relation as a line passing through the origin.

Considering the curved spectral shape measured in the previous section, and fixing the curvature at $\beta = 0.50$, we can calculate the shift in E_{max} necessary to cause the observed maximum change in R. The variation is of the order of 400 GeV, which is fully compatible with the results of the previous section seen in the final column of Table 1.

6. Hard X-ray and γ-ray correlation

During the April 1997 multi-wavelength campaign, Mkn 501 was observed from X-ray to VHE energies (e.g., see Catanese et al. 1997). In the energy range 0.1–200 keV, the BeppoSAX satellite observed for three periods of ~10 hours: on April 7th, 11th and 16th (Pian et al. 1998). The RXTE satellite observed in the 2–80 keV range (Lamer & Wagner 1998) between July 11th and 16th. X-ray and high energy γ-ray observations were also performed by the OSSE and EGRET instruments respectively, on board CGRO. In the VHE regime, CAT, HEGRA, Whipple and other instruments were active (Protheroe et al. 1997).

In the X-ray range, extremely hard spectra were reported by BeppoSAX indicating that the synchrotron power output peaked at 100 keV or more. OSSE observations gave similar conclusions (Catanese et al. 1997).

The highest-intensity TeV flare recorded by CAT in 1997 occurred on April 16th (see Fig. 1), where CAT and BeppoSAX observations overlapped for about ten minutes, providing some simultaneous VHE γ-ray and X-ray data. The observation logs are given in Table 3. On April 7th and 11th, the source was less bright and only quasi-simultaneous data were available, as there was a delay of about two hours between CAT and BeppoSAX pointing periods. However, data from all Čerenkov
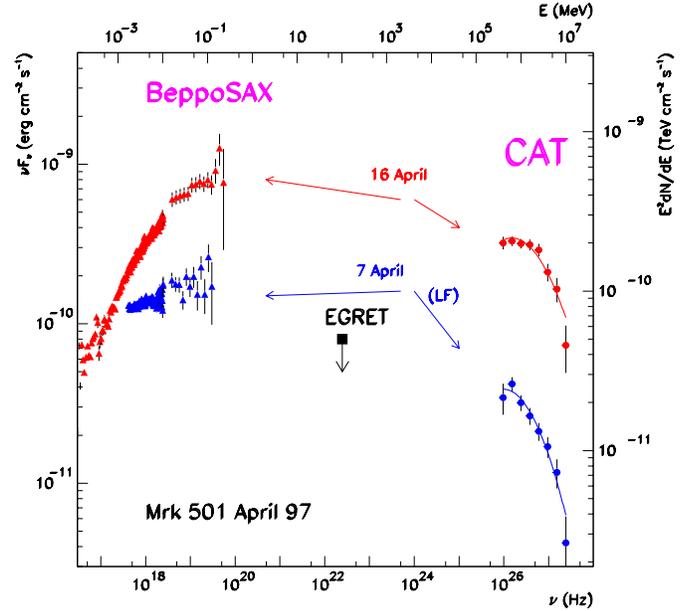

Fig. 6. X-ray and VHE spectra given as νF_ν. For April 7th and 16th, BeppoSAX data are from Pian et al. (1998). The LF subset in CAT was used to represent the spectrum corresponding to April 7th. The EGRET upper limit is taken from Samuelson et al. (1998) and corresponds to observations between April 9th and 15th.

telescopes (CAT, Whipple and HEGRA) show no large variations in source flux for the periods 5th to 9th and 10th to 12th (Protheroe et al. 1997). Hence, γ-ray and X-ray levels can be considered as simultaneous data and compared in a reliable manner.

Table 3 shows comparisons of the VHE and X-ray power output from BeppoSAX and CAT data. The ratio of VHE to X-ray power outputs is plotted in Fig. 5 as a function of the X-ray power, and clearly increases with source brightness.

The spectra are shown in Fig. 6. Because of the very high intensity of the source on April 16th, it is possible to derive its spectrum for that single observation (one and a half hours of data). In order to represent the spectrum corresponding to April 7th, the LF data-subset comprising runs with similar flux levels (within 30%) was used.

Four characteristics come out of these comparisons:

(i) the fluxes and SED shapes seen in the CAT and BeppoSAX data, together with the EGRET upper limit in the GeV domain, imply a double structure in the power output of Mkn 501;

(ii) hard X-rays and VHE γ-rays show correlated variability;

(iii) the luminosity in X-rays remains higher than in γ-rays;

(iv) during the flares, the VHE intensity recorded by CAT increased by a larger factor than the X-ray intensity recorded by BeppoSAX (Table 3). Therefore, the ratio of VHE to X-ray intensities increased with source brightness (Fig. 5).

7. Discussion

CAT observations of Mkn 501 during 1997 have revealed several spectral properties: a curved shape and an emission extending above $10\,\mathrm{TeV}$ (Sect. 4), hardness–intensity correlations (Sect. 5), X-ray and γ-ray correlations (Sect. 6). Together with the power deficit in the GeV range, this strongly suggests a two-component emission spectrum for Mkn 501.

It is generally accepted that the high luminosity of blazars ($\sim 10^{45-48}$ erg/s) requires a relativistically-amplified beamed-emission. Beaming is also required for the source to be transparent to γ-rays if both VHE and IR to UV emissions originate in the same region of the jet (Dermer & Gehrels 1995; Dondi & Ghisellini 1995). Two major processes have been suggested as the dominant source of the high-energy emission from blazars: inverse Compton (IC) scattering of low-energy photons by ultra-relativistic electrons, and π^0-decay through photo-production or secondary production of pions by an ultra-high-energy hadronic component in the jet (Mannheim & Biermann 1992; Mannheim 1993).

In the IC case, a double-structure spectrum in terms of synchrotron and IC emissions is predicted with the two components being correlated in intensity, hardness, energy of the peak luminosities, etc. The correlations depend on the nature of the target-photon population. This may consist of either synchrotron photons within the jet – the synchrotron self-Compton, or SSC, mechanism (Königl 1981; Marscher & Gear 1985; Ghisellini et al. 1996) – or external radiation, either from the accretion disk (Sikora et al. 1994; Dermer et al. 1992), or reflected by the broad-line region clouds (Ghisellini & Madau 1996). Spectral variations of the primary electrons (due for example to a change in the injection-acceleration efficiency or in cooling conditions), seen through their effect on the synchrotron radiation, should be reflected in the high-energy emission, especially when the IC interactions take place in the Thomson limit. In the Klein-Nishina regime, hardening effects can be attenuated because of a severe cross-section drop at high energies.

In hadronic models, no particular predictions are made for a marked two-component emission. A continuum emission is predicted due to secondary cascades produced by hadronic interactions of ultra-high-energy protons, which tend to fill the gap between the high-energy (γ-ray) and low-energy (X-ray) domains.

7.1. Curved shape

The spectral shape derived in Sect. 4 between $330\,\mathrm{GeV}$ and $13\,\mathrm{TeV}$ is clearly curved. This curvature is in contrast with reports on the other TeV blazar, Mkn 421, whose spectrum has been observed to be compatible with a power-law (Krennrich et al. 1999; Piron et al., in preparation). The curved shape is predicted by IC models of blazar spectra but can only be seen if the IC component is observed over a broad dynamic range close to the maximum power emission energy (i.e., close to the maximum of the IC bump in a νF_ν representation). The curvature could arise from intrinsic absorption effects (within the jet or due to nearby radiation fields, from the accretion disk, for example) and/or from a cutoff in the primary particle spectrum. However, when observing within a limited energy range – as compared to the energy scale over which the emission phenomenon is taking place – not including the peak emission region, a power-law spectrum is naturally seen. We note that the reported synchrotron peak of Mkn 501 during 1997 is well above that of Mkn 421 ($\sim 100\,\mathrm{keV}$ as compared to $\sim 1\,\mathrm{keV}$) and that the IC and synchrotron peak-emission energies are expected to be correlated in IC schemes. This correlation has also been established on a purely observational basis using a large sample of blazars (Fossati et al. 1998). Thus, the difference in observed spectral shapes for Mkn 421 and Mkn 501 may well arise because the peak of the high-energy component for Mkn 421 is below the VHE energy domain, whereas the peak for Mkn 501 is well above our threshold.

The overall spectrum, and particularly the highest energy γ-rays (10–20 TeV), may be affected by intergalactic absorption due to pair creation on the intergalactic background IR radiation (Stecker & de Jager 1998; Biller et al. 1998). Therefore any interpretation of VHE spectra in terms of emission models should take this effect into account. It could be disentangled from intrinsic absorption features if we dispose of a large sample of VHE emitters. Nevertheless, the different spectral shapes of Mkn 501 and Mkn 421 – which have similar red-shifts and have been detected above $10\,\mathrm{TeV}$ (Krennrich et al. 1999) – imply already that the curvature of the former must be mainly due to intrinsic features.

7.2. Hardness–intensity and γ-ray/X-ray correlations

In Sect. 5, a correlation between VHE intensity and spectral hardness was demonstrated. If we assume a constant curvature for different-activity states as indicated by the data, this effect is equivalent to an increase of approximately $400\,\mathrm{GeV}$ for the peak emission energy E_{max} for an intensity change of about an order of magnitude between the LF and HF subsets.

BeppoSAX results have established that the energy of the maximum power output during the active period is much larger than during the low-emission state (Pian et al. 1998). A comparison of April 7th and 16th X-ray data suggests that this hardening continues as the intensity increases during the flare.

This simultaneous observation of flaring activity and spectrum hardening, in both X-ray and VHE energy ranges, is naturally explained by a common primary electron population, as expected in the framework of inverse Compton models. Pian et al. (1998) claim that a significant change in the magnetic field intensity or the Doppler factor is unlikely since the expected

changes in the lower-energy part of Mkn 501 spectrum which would result have not been observed; i.e., the X-ray emission below $0.5\,\mathrm{keV}$ did not show any dramatic variation. In this case, this would leave the injection of a transient electron population and/or a change in the acceleration efficiency (an increase of the maximum energy of electrons) as the most likely source of the flares.

In the framework of IC models, the observed increase of the VHE to X-ray intensity ratio with source brightness (see Fig. 5) is qualitatively in agreement with the SSC mechanism which predicts a quadratic increase of VHE intensity with X-ray brightness due to the fact that both the electron population and the "target" synchrotron populations are enhanced. The yield of the SSC contribution to the IC process should be damped by the decreasing cross-section in the extreme relativistic Klein-Nishina regime. The highest intensity data point in Fig. 5 is consistent with such an effect.

7.3. Comparison with other VHE detections

The Whipple group's results for Mkn 501 between 300 GeV and 10 TeV (Samuelson et al. 1998) show an average spectrum with $\alpha = 2.20 \pm 0.04^{\mathrm{stat}} \pm 0.05^{\mathrm{syst}}$ and $\beta = 0.47 \pm 0.07^{\mathrm{stat}}$, in good agreement with CAT results within the statistical errors. HEGRA (Aharonian et al. 1999) has also demonstrated a curved spectral shape. Given the source variability and the different source sampling due to local conditions, one does not expect the absolute flux levels observed in the three experiments to be identical. Nonetheless, the convergence of these three observations as regards the spectral *shape* is noteworthy.

No hardening effect has been claimed by either Whipple or HEGRA. While this appears to contradict the effect seen in our data, it may be explained for each case. We note that Whipple's reported results are limited to the period between February and June 1997 and include 21.1^{h} of data. The CAT results are based on a larger sample (40.5^{h} of observations for the hardness-intensity studies), and include runs from June to October 1997, providing large statistics of the source emission in a lower-activity state. The effect reported here could hardly be seen with lower statistics.

Considering HEGRA results, their higher energy threshold might well result in a lower sensitivity to the hardness-intensity correlation: as shown in Sect. 6, this effect becomes less significant when we consider higher energy events.

8. Conclusion

The results reported in this paper are based on the large sample of data taken by CAT from March to October 1997, including periods with very different source intensities. The Mkn 501

spectrum has been measured from $330\,\mathrm{GeV}$ to $13\,\mathrm{TeV}$. The curvature reported by the Whipple group is confirmed. In addition, CAT data show an intensity-hardness correlation which can be simply described by a shift of the peak TeV emission energy.

The overall picture emerging from these spectral properties and from the comparison with simultaneous and quasi-simultaneous BeppoSAX observations favours the interpretation in terms of an energetic electron beam propagating in a magnetic plasma and producing X-rays through synchrotron radiation as well as VHE γ-rays through inverse Compton scattering of low-energy photons.

References

Aharonian F., et al., 1999, A&A 342, 69
Barrau A., et al., 1998, NIM A416, 278
Biller S., et al., 1998, Phys. Rev. Lett. 80, 2992
Bradbury S., et al., 1997, A&A 320, L5
Catanese M., et al., 1997, ApJ 487, L143
Ciliegi P., Bassani L., Caroli E., 1995, ApJ 439, 80
Dermer C.D., Gehrels N., 1995, ApJ 447, 103
Dermer C., Schlickeiser R., Mastichiadis A., 1992, A&A 256, L27
Dondi L., Ghisellini G., 1995, MNRAS 273, 583
Fossati G., Maraschi L., Celotti A., Comastri A., Ghisellini G., 1998, MNRAS 299, 433
Ghisellini G., Madau P., 1996, MNRAS 280, 67
Ghisellini G., Maraschi L., Dondi L., 1996, A&AS 120, 503
Königl A., 1981, ApJ 243, 700
Krennrich F. et al., 1999, ApJ 511, 149
Lamer G., Wagner S., 1998, A&A 331, L13
Le Bohec S., et al., 1998, NIM A416, 425
Mannheim K., 1993, A&A 269, 67
Mannheim K., Biermann P., 1992, A&A 253, L21
Marscher A., Gear W., 1985, ApJ 298, 114
Pian E., et al., 1998, ApJ 492, L17
Piron F., et al., 1999, in preparation
Protheroe R.J., et al., 1997, Proc. 25$^{\mathrm{th}}$ ICRC (Durban) Vol. 8, p. 317
Quinn J., et al., 1996, ApJ 456, L83
Samuelson F., et al., 1998, ApJ 501, L17
Sikora M., Begelman M., Rees M., 1994, ApJ 421, 153
Stecker F., de Jager O.C., 1998, A&A 334, L85
Stickel M., Padovani P., Urry C.M., Fried J.W., Kühr H., 1991, ApJ 374, 431